

## CARACTERIZAÇÃO DE REVESTIMENTOS DE FOSFATO DE CÁLCIO, PRATA E MAGNÉSIO EM SUBSTRATOS DE IMPLANTES BIOMÉDICOS DE TITÂNIO PELO MÉTODO DE ASPERSÃO POR CHAMA.

## CHARACTERIZATION OF CALCIUM PHOSPHATE, SILVER, AND MAGNESIUM COATINGS ON TITANIUM BIOMEDICAL IMPLANT SUBSTRATES BY FLAME SPRAY METHOD.

Noora Jameel Hintaw \*

University of Kerbala, College of Science, Physics Department. Iraq

Mohammed Abdul Hur Kadhim

University of Kerbala, College of Science, Physics Department. Iraq

Muhanned Salah Abdul Sattar

University of Kerbala, College of Dentistry. Iraq

\* Noora Jameel Hintaw

e-mail:nora.j@s.uokerbala.edu.iq

Received 26 July 2024; received in revised form 05 February 2025; accepted 08 February 2025

### RESUMO

**Introdução:** Neste trabalho, o comportamento do fosfato de cálcio (CaP) como revestimento em bases de titânio (Ti-6Al-4V) foi investigado como um material compósito para prata e magnésio e prata e magnésio juntos usando tecnologia de pulverização de chama. **Objetivo:** Caracterização de revestimentos de fosfato de cálcio, prata e magnésio em substratos de implantes biomédicos de titânio. **Métodos:** usando tecnologia de pulverização de chama. **Resultados e Discussão:** Hidroxiapatita (HAP) foi observada em todas as camadas de revestimento e picos extras foram observados para a prata e magnésio nos padrões de XRD (difração de raios X) das camadas revestidas. A espessura das camadas de revestimento foi de (107,8, 108,7, 106,5, 206,7) nm e o tamanho médio do grão foi de (44,12, 43,80, 44,6, 34,92) nm para fosfato de cálcio, fosfato de cálcio e prata, fosfato de cálcio e magnésio, fosfato de cálcio, prata e magnésio juntos, respectivamente. Quanto às medidas do ângulo de molhabilidade, foi de 50,101 graus para o substrato Ti6Al4V e 8,886 graus para fosfato de cálcio como revestimento e para outras camadas de revestimento, foi igual a zero. Quanto às medidas do teste de adesão, todas as amostras foram menores que 5%, significando uma classificação B4 de acordo com a ASTM. Da mesma forma, a análise por espectroscopia de raios X de dispersão de energia (EDX) mostra a presença de Ca, P, Ag e Mg. no XRD (difração de raios X) fica claro que a severidade dos picos aumentou para (Ca P Ag Mg). Em contraste, uma diminuição na largura dos picos significa o maior grau de cristalinidade e crescimento de cristalito. A morfologia da nanoestrutura é exibida nas imagens de microscopia eletrônica de varredura de emissão de campo, e a morfologia da superfície dos revestimentos é mostrada como o formato das partículas. O ângulo de contato diminuiu porque os revestimentos contribuíram para uma maior absorção de água e reduziram o ângulo de contato, a partir do teste de adesão, a camada de revestimento tem uma boa ligação à superfície do substrato. **Conclusões:** Essas propriedades da camada de revestimento têm a capacidade de melhorar tanto a biocompatibilidade quanto a bioatividade dos implantes médicos protéticos, aumentando assim a capacidade de osseointegração.

**Palavras-chave:** *Implante biomédico, titânio, spray de chama.*

### ABSTRACT

**Background:** In this work, the behavior of calcium phosphate (CaP) as a coating on titanium (Ti-6Al-4V) bases was investigated as a composite material for both silver and magnesium and silver and magnesium together using flame spray technology. **Aims:** characterization of calcium phosphate, silver, and magnesium coatings on titanium biomedical implant substrates. **Methods:** using flame spray technology. **Results:** Hydroxyapatite (HAP) was observed in all coating layers, and extra peaks were observed for the silver and magnesium in the XRD (X-ray diffraction) patterns of the coated layers. The thickness of the coating layers was (107.8, 108.7, 106.5, 206.7) nm. and the average grain size was (44.12, 43.80, 44.6, 34.92) nm for calcium phosphide, calcium phosphide and silver, calcium phosphide and magnesium, calcium phosphide, silver and magnesium together, respectively. As for wettability angle measurements, it was 50.101 degrees for the Ti6Al4V substrate and 8.886 degrees for calcium phosphide as a coating, and for the other coating layers, it was equal to zero. As for the

adhesion test measurements, all samples were less than 5%, meaning a B4 classification according to ASTM. Likewise, energy-dispersive X-ray spectroscopy (EDX) analysis shows the presence of Ca, P, Ag, and Mg. **Discussion:** In the XRD (X-ray diffraction), it's clear that the severity of the peaks increased for (CaP Ag Mg). In contrast, a decrease in the width of the peaks signifies the highest degree of crystallinity and crystallite growth. The morphology of the nanostructure is displayed in the field emission scanning electron microscopy pictures, and the surface morphology of the coatings is shown as the shape of the particles. The contact angle decreased because coatings contributed to greater water absorption and reduced the contact angle. From the adhesion test, the coating layer has a good bond to the substrate surface. **Conclusions:** These coating layer properties can improve both the biocompatibility and bioactivity of prosthetic medical implants, thus enhancing the osseointegration capacity.

**Keywords:** *Biomedical Implant, Titanium, Flame Spray.*

---

## 1. INTRODUCTION:

Biomedical implants are made of metals and their alloys due to their superior mechanical qualities, acceptable biocompatibility, and ease of production. However, breakdown occurs when these elements are utilized in an environment where human tissue is extremely corrosive. A bioactive coating applied to the surface of metallic implants may offer an alluring remedy for the deterioration issues. Additionally, this will enhance bone formation in order to ensure a successful implantation. Surface coatings alter the shape, structure, and content of the biomaterials' surfaces while maintaining their bulk mechanical characteristics (Hanawa, 2005). An inorganic substance, bone is composed of hydroxyapatite (HA), a mineral compound that makes up 65% to 70% of the material, and additional elements like magnesium, zinc, iron, and fluoride that makeup 30% to 35%. Biomedical uses of hydroxyapatite include dental implants, orthopedic devices, tissue engineering, and bioactive coatings (Sygnatowicz and Tiwari, 2009).

Recently, studies have attracted a lot of interest in calcium phosphate materials because they are chemically comparable to teeth and bones. The nontoxicity of their chemical constituents and their superior biocompatibility make them appealing biological materials (Epple *et al.*, 2010; Hench, 1991). Hydroxyapatite and tricalcium phosphate are the two most commonly used calcium phosphates and constitute a class of bioactive synthetic materials. Because of their osteoconductivity, chemical similarity to the skeletal tissue, and crystalline structures, these types are frequently used (Hench, 1991; LeGeros, 1988).

In order to integrate the bioactivity of calcium phosphates (CaP) with the strength of the titanium, coatings made of titanium and titanium alloy are also utilized (Geesink, 2002; Barrère *et al.*, 2003).

In order to integrate the bioactivity of calcium phosphates (CaP) with the strength of the titanium, coatings made of titanium and titanium alloy are also utilized. Biocompatible coatings are the best choice for metallic implants. In addition to increasing the bioactivity of the metal surface, coatings can work as barriers between the metal substrate and its surroundings (Brown *et al.*, 2015). Magnesium (Mg) and its alloys seem to be the most desirable of these metals because they are non-toxic and have mechanical qualities that are close to those of bones when compared to other metals. Magnesium-based metallic implants are biocompatible and lightweight, which gives them various advantages over other implantable metals currently in use.

Among these are the removal of the stress shielding and the fact that a second procedure is not required following a metal implant (Brown *et al.*, 2015). It is regarded as a low-density metal (Jacobs *et al.*, 1998). Compared to these implants, magnesium has the advantage of potentially reducing stress shielding. Due to magnesium's ability to biodegrade, if the pace of corrosion is managed, the metal will gradually deteriorate and eliminate the need for additional removal procedures, lowering health risks, expenses, and scars. It has been established that the patient may benefit from the corrosion products of magnesium. Other metals, on the other hand, displayed harmful corrosion products (Agins *et al.*, 1988), which adds to the benefits of magnesium as a substrate.

In the medical field, one of the most used metals for plating is silver. The antibacterial properties of silver metal are strong. Silver ions cause mayhem inside bacteria by creating holes in their membranes, which is how they carry out their lethal function. Long-term antibacterial efficacy owing to sustained ion release, low toxicity, and good biocompatibility with human cells (Slenters *et al.*, 2008).

Ti-6Al-4V This alloy has extensive

applicability in both industrial and biomedical domains (Handbook, 1990). Aluminum functions as a stabilizer of the  $\alpha$  phase in this material, preventing its hot production, while vanadium stabilizes the  $\beta$  phase, increasing the material's mechanical resilience to heat treatment and aging (Handbook, 1990; Copete *et al.*, 2017). Because of its high fatigue limit, bio-inertness, ability to integrate Osseo and resistance to corrosion from body fluids, titanium is regarded as the most biocompatible metal.

The biological response (cell adhesion and proliferation) to a biomaterial is largely determined by its surface characteristics. Osseo integration is aided by titanium's ability to stimulate angiogenesis because of its high surface energy and microstructure (Raines *et al.*, 2010).

The thermal spray-to-flame (FS) method is inexpensive, adaptable, and simple to use. It also makes it possible to create coatings that satisfy the requirements for crystallinity, adhesion, and porosity that are needed in biomedical applications. Ceramics having a high melting point are among the many materials that can be coated using flame spray technology.

The shape and chemical makeup of the powders, the substrate's preparation and composition, the spray distance, the gas ratio (oxygen:acetylene), and the flow of feed powders are some of the variables that affect the morphology of the coating layer produced by thermal flame. The advice of powder producers, the experimenter's expertise, and the outcomes of numerical simulations are taken into consideration while organizing the coating's preparation (Ferrer *et al.*, 2018). The aims of this study are the characterization of calcium phosphate, silver, and magnesium coatings on titanium biomedical implant substrates to improve both the biocompatibility and bioactivity of prosthetic medical implants, thus enhancing the osseointegration capacity.

## 2. MATERIALS AND METHODS:

### 2.1. Materials

Calcium phosphate ( $\text{Ca}_3(\text{PO}_4)_2$ ) (Merck Co.), Titanium (Ti-6Al-4V), which is a proprietary product of Baoji Jensheng, China; silver and magnesium powder (AVOCHEM, UK) ethanol solution and acetone 99.8% (Scharlue, ESPAIN).

## 2.2. Experimental procedures

### 2.2.1. Substrate Preparation

The Ti-6Al-4V ELI material with a diameter of 18 mm and thickness of 2 mm was used as a substrate for the study. The rough surface of the material was then reduced by a grinding process using sandpaper with mesh sizes of 80, 300, and 500. The sample was then cleaned by soaking it using ethanol solution for 15 minutes and acetone for 15 minutes in an ultrasonic bath (Sonomatic, Germany) model 170-2-T80.

### 2.2.2. Deposition coatings by flame spray method

Cap coatings were deposited by thermal spraying equipment (Eutectic and Castolin) on Ti-6AL-4V specimens, which is a proprietary product of Baoji Jensheng, China. In this system, acetylene and oxygen were used as combustion gases, and the air was used as the carrier gas to feed the HA powder from the hopper to the spray torch.

This system is a high-velocity version of a flame spraying system and is specially designed for ceramic coatings. The temperature of oxyacetylene flames in the CERAJET system is 2700 °C. The spray parameters at a spray distance of 12 cm were an oxidizing atmosphere with a ratio of 1:3.2, six preheating passes for the substrate, and three spray passes. Deposition of calcium phosphate was performed on a heated Ti-6Al-4V substrate. Magnesium powder with 5% concentration was mixed with the 95% calcium phosphate, then silver powder with 5% concentration was mixed with the 95% Calcium phosphate, and deposition on a heated Ti-6Al-4V substrate was performed. Finally, magnesium 5% concentration powder was mixed with the 90% calcium phosphate and deposited.

### 2.2.3. Analysis techniques

By X-ray diffraction (XRD) (Shimadzu XRD 6000), the microstructure of powders and coatings was acquired, and by using an optical microscope (MIRA3 TE-SCAN), the microstructure observations were conducted. E-SEM measured the thickness of the coatings.

The surface chemical composition was determined with an energy-dispersive X-ray (EDX) detector. By a cross-cut tape test, the strength of the coating layer adhesion on the surface of the substrate was determined and established based on the American Society for

Testing and Materials ASTM D3359-17 standard (Tape, 2017). Also, wettability angle measurements are made by an optical contact angle meter, the Lite (TL 100 and TL. 101) (USA) of a CCD camera called an optical tensiometer.

### 3. RESULTS AND DISCUSSION:

#### 3.1. RESULTS

##### 3.1.1. Structural properties

The X-ray diffraction (XRD) patterns for the deposited layers (Cap, Cap Ag, Cap Mg, Cap Ag Mg) were obtained using flame coating for the substrate. In Figure 1 the sample showed phase hydroxyapatite (HA) matched with standard card (09-0432) with multiple peaks that matched with lattice planes appearing at (100), (021), (200), (002), (041), (100), (310), (311), (222), (312), (304) and (513) at different diffraction angles.

Figure 2 showed x-ray diffraction patterns for calcium phosphide and silver as a coating (Cap Ag). The sample showed phase hydroxyapatite (HA) matched with the standard card (09-0432). multiple peaks that match the lattice planes appeared (110), (002), (210), (211), (111), (310), (222), (213) and (004), (510) at different diffraction angles, and additional peaks for the silver matched with standard card (04-0783) peaks appeared corresponding to the lattice planes (111), (200), (220), (311).

Also, the calcium phosphide and magnesium as a coating (Cap Mg) orifice are shown in Figure 3. The sample showed hydroxyapatite (HA) matched with the standard card (09-0432); multiple peaks that matched with the lattice planes appeared at (110), (111), (002), (200), (211), (310), (222), (213), (004), (313), (214), (502), and (512) at diffraction angles, and additional peaks for the magnesium appeared in the sample matched with the standard card (35-0821); peaks appeared corresponding to the lattice planes (002) and (101).

The XRD (X-ray diffraction) patterns of the coated layers for (Cap Ag Mg) are shown in Figure 4. The sample showed phase hydroxyapatite (HA) matched with the standard card (09-0432). multiple peaks that match the lattice planes appeared (110), (111), (002), (210), (200), (310), (222), (213), (004), and (313) at diffraction angles, and peaks for the silver appeared in the sample matched with the standard card (04-0783). peaks appeared corresponding to the lattice planes (111), (220), and (311), and peaks for magnesium appeared in the sample matched with standard card (35-0821); peaks appeared corresponding to the

lattice planes (002), (101), (200), and (201).

##### 3.1.2. The Field Emission Scanning Electron Microscopy (FE-SEM)

The morphology of the nanostructure is displayed in the field emission scanning electron microscopy pictures. The surface morphology of the coatings is shown in Figure 5 (a, b, c, and d) (Cap, Cap Ag, Cap Mg, Cap Ag Mg). The sample surfaces vary in the shapes of nanostructures. The shape of the particles is mainly spherical in all of the obtained specimens, and the thickness was measured by analyzing the FE-SEM picture and gave values of 107.8 nm, 108.7 nm, 106.5 nm and 206.7 nm for (Cap, Cap Ag, Cap Mg, Cap Ag, Mg) respectively, and the average grain size was (44.12, 43.80, 44.6, 34.92) nm for calcium phosphide, calcium phosphide and silver, calcium phosphide and magnesium, calcium phosphide, silver, and magnesium together, respectively.

##### 3.1.3. Energy Dispersive (X-Ray) Spectroscopy (EDX)

**Table 1.** Show concentration of the elements EDX analysis for titanium substrate coated with (Cap, Cap Ag, Cap Mg, Cap Ag Mg).

Substrate	Items	Element	Weight %
Titanium	Cap	O	24.9
		P	32.1
		Ca	42.1
		Ti	0.7
	Cap Ag	O	28.4
		P	29.0
		Ca	37.7
		Fe	0.4
		Ag	4.2
	Cap Mg	O	26.2
		Mg	4.1
		P	31.0
		Ca	38.1
		Ti	0.5
	Cap Ag Mg	O	14.5
		Mg	4.1
P		33.5	
Ca		43.3	
Ti		0.2	

The contents of dispersive X-ray spectroscopy elements are analyzed using energy. In an electron microscope, electrons are utilized instead of light. In an optical microscope, electromagnetic lenses focus and accelerate the electron. X-rays are emitted with various energies depending on the properties of the electronic transition of elements. Figure (6, 7, 8, 9) shows

EDX compositional analysis for the Ti-6Al-4V substrate coated with (Cap, Cap Ag, Cap Mg, and Cap Ag Mg), respectively. Table 1 lists the concentration of the elements. We note that Ca, P, Ag, and Mg elements appeared. Also, the concentration of the element (Ti) appeared in samples in a very small percentage.

### 3.1.4. The Adhesion Test

To evaluate the bond strength, the tensile test is used in accordance with ASTM D3359-17, a standard developed for testing the adhesion strength of coatings to surfaces. This standard is known as "Standard Test Methods for Rating Adhesion by Tape Test" and is used to determine the adhesion of a coating to a given surface. The adhesion strength of the coating was evaluated using the cross-hatch method as described in ASTM D3359-17. In accordance with ASTM D3359-17 guidelines, the coating adhesion test using tape was applied to the surface of the sample. The adhesion test measurements for all samples were less than 5%, meaning a B4 classification according to the coating adhesion scale specified in ASTM D3359-17 (Tape, 2017), indicating strong adhesion with minimal peeling, as shown in Figure 10. The results obtained were in accordance with the requirements of ASTM D3359-17, confirming the adhesion efficiency of the coating used. For biological applications, the coating layer's strength of adhesion to the substrate is an essential characteristic.

### 3.1.5. Wettability (Contact Angel) Test

The wettability (contact angle) tests for the Ti-6Al-4V substrate uncoated and coated with (Cap, Cap Ag, Cap Mg, Cap Ag Mg), respectively, show that the contact angle decreases with coating and reaches zero degrees for samples coated with (Cap Ag, Cap Mg, Cap Ag Mg) compared with 8.886 degrees for the substrate coated (Cap) and with 50.101 degrees for the uncoated sample as shown in Table 2.

**Table 2.** Wettability contact angle test for titanium substrate coated with (Cap, Cap Ag, Cap Mg, Cap Ag Mg).

Item	Contact Angle (degree)
Ti base	50.101
Ti-cap	8.886
Ti-cap-Ag	0.00
Ti-cap-Mg	0.00
Ti-cap-Ag-Mg	0.00

## 3.2. Discussion

The X-ray diffraction (XRD) patterns for the deposited layers appeared. In Figure 1 appeared phase hydroxyapatite (HA) and multiple peaks that match the lattice planes appeared at different diffraction angles, which confirms the hexagonal HA structure (Mahabole *et al.*, 2005; Vaidhyanathan and Rao, 1996; Gómez-Morales, 2001).

Figure 2 shows phase hydroxyapatite (HA), and multiple peaks that match the lattice planes appeared at different diffraction angles, and peaks for the silver appeared. As observed in the XRD analysis of the obtained coatings, the absence of some silver peaks in the diffraction patterns is attributed to the low concentration of Ag used in the coatings (Yanovska *et al.*, 2014).

In Figure 3 appeared, multiple peaks for hydroxyapatite that matched the lattice planes appeared at different diffraction angles and appeared peaks for the magnesium; the diffraction peaks with the addition of Mg did not shift to lower  $2\theta$  values (Wang *et al.*, 2020). Additionally, Mg addition into the HAP lattice would impact the HAP thermal stability and crystallization, enhancing the formation of  $\beta$ -TCP (Stipiecec *et al.*, 2014).

Figure 4 shows multiple peaks for hydroxyapatite that match the lattice planes that appeared at different diffraction angles and peaks for silver and magnesium. The little shifts in the positions of peaks due to lattice strain are the outcome of crystalline size variations or lattice flaws (Hazaa, 2015). Additionally, the severity of the peaks increased for (Cap Ag Mg). In contrast, a decrease in the width of the peaks signifies the highest degree of crystallinity and crystallite growth.

The field emission scanning electron microscopy pictures (FE-SEM) shown in Figure 5 (a, b, c, and d) show that in Figure 5a, the splat is observed with a little splash, producing a uniform coating with some unmelted particles that combine with other fully melted particles to form a coating with low porosity. In Figure 5b, as observed in part (a), the sample looked to be coated in bulk, and some nanoparticles were also attached. These samples showed porosity and some interlamellar cracks, which are caused by the residual stress due to thermal shock and which contribute significantly to the porosity.

In Figure 5c, the observed sample looked to be coated in bulk, and also, to attach some nanoparticles, greater agglomerates, and some surface porosity are seen.

In Figure 5d, the sample (Cap Ag Mg) appeared as a distinctive sample of nanostructures uniformly distributed, forming a high porosity structure. Therefore, calcium phosphide coating with silver and magnesium together has a better covering of hydroxyapatite (HAP) with a thickness of 206.7 nm and an average grain size of 34.92 nm without agglomeration and cracks.

In the same way, it can be seen that the coating has a uniform distribution of HAP, which completely covers the substrate surface.

Also, some porosity and bigger agglomerates on the surface are noticed; this agglomeration is owing to the increasing thickness of the layer (Venkatesan and Kim, 2010). The porous surface enhances fixation via the growth of bone into the coating and creates a mechanical interlock alloy (Takács, 2005).

Figures (6, 7, 8, and 9) show EDX compositional analysis for the Ti-6Al-4V substrate coated. We note that Ca, P, Ag, and Mg elements appeared. In general, from Table 1, the reduction in the quantity of the weight concentrate of titanium element does not appear in some samples due to the uniform coverage of the substrate by the layer of Hap. This leads to an increase in the thickness of the layer.

The form of Hydroxyapatite is  $\text{Ca}_{10}(\text{PO}_4)_6(\text{OH})_2$ . where the weight concentrate of calcium (Ca) is more than phosphorus (P). Certain researchers proposed that during the sputtering, the calcium atoms, which have a little more mass, displace the atoms of less mass, especially phosphorus atoms, on the surface (Pichugin *et al.*, 2006).

The source of the oxygen comes from the HAp and is also a result of the exposure of samples to air and heat of sputtering techniques. This good feature increases air cavities or pores for compatibility with tissue bone and increases corrosion resistance. From the EDX patterns in Table 1, it can be concluded that calcium (Ca) and phosphorus (P) concentrations on the Ti-6Al-4V substrate coated (Cap Ag Mg) are higher than in other samples.

In Figure 10, the coating of various materials on the titanium surface tends to bond strongly to the titanium surface and shows the least peeling area.

There is a need for a strongly adhered hydroxyapatite (HAP) coating on the surface of the material to preserve the functional and structural role of the coating throughout the

process of implantation.

When in contact with bodily fluids, the hydroxyapatite coating structurally works as a barrier to prevent the release of toxic elements from the component into the biological environment and to prevent corrosion (Cavalli *et al.*, 2001). The hydroxyapatite coating's functional role involves the body's metabolism, which causes the formation of bone tissue. The hydroxyapatite layer forms a direct link with bone tissue without fibrous tissue involvement in implant material and interfacial tissue. Implant looseness may result from the fibrous tissue encapsulating the implant material. (Kokubo and Takadama, 2006; Suchanek *et al.*, 2015). The contact angle decreased because coatings contributed to greater water absorption and reduced the contact angle, as shown in Table 2. In other words, (Cap, Cap Ag, Cap Mg, and Cap Ag Mg) coatings significantly increase the hydrophobicity of the Ti6A14V samples in comparison with the uncoated samples. These results agree with the study (Kadhim *et al.*, 2022).

#### 4. CONCLUSIONS:

The thermal flame spray technique was utilized to produce a hydroxyapatite (HAP) coating on the surface of the Ti-6Al-4V substrate. Variations in the addition of chemical ingredients affect the surface properties, such as adhesion strength, particle size, wettability, and layer thickness and coverage. The results of the tests indicated that the deposited layers had good qualities and could be utilized for coating medical implants. The crystal structure of hydroxyapatite was revealed via X-ray diffraction, and the phase hydroxyapatite appeared. The surface exhibited a high porosity and compact shape, with a thickness of 206.7 nm for the (Cap Ag Mg) coating, as demonstrated by the FESEM images. The wettability test showed that the contact angle decreased, and hydrophilic surfaces were created.

Coating layer properties have the ability to improve the biocompatibility of medical implants, thus enhancing the osseointegration capacity.

#### 5. DECLARATIONS

##### 5.1. Study Limitations

There were limitations at the time of the study, namely the difficulty of the coating method in obtaining a homogeneous and porous coating and the difficulty of obtaining and cutting titanium

in rod form.

## 5.2. Acknowledgements

I want to express my most tremendous gratitude and appreciation to my supervisors, Dr. Mohammed Abdul Hur Kadhim and Dr. Muhanned Salah Abdul Sattar, for their guidance and suggestions throughout the research. I would also like to thank my colleagues and everyone who has helped.

## 5.3. Funding source

The authors funded this research. In accordance with the ethical guidelines of the Periódico Tchê Química, which do not allow donations from authors with manuscripts under evaluation (even when research funds are available), or in cases of authors' financial constraints, publication costs were fully absorbed by the journal under our Platinum Open Access policy, through the support of the Araucária Scientific Association (<https://acaria.org/>). This policy aims to ensure complete independence between the editorial process and any financial aspects, reinforcing our commitment to scientific integrity and equity in knowledge dissemination.

## 5.4. Competing Interests

The authors declare that no potential conflict of interest existed in this publication.

## 5.5. Open Access

This article is licensed under a Creative Commons Attribution 4.0 (CC BY 4.0) International License, which permits use, sharing, adaptation, distribution, and reproduction in any medium or format, as long as you give appropriate credit to the original author(s) and the source, provide a link to the Creative Commons license, and indicate if changes were made. The images or other third-party material in this article are included in the article's Creative Commons license unless indicated otherwise in a credit line to the material. If material is not included in the article's Creative Commons license and your intended use is not permitted by statutory regulation or exceeds the permitted use, you will need to obtain permission directly from the copyright holder. To view a copy of this license, visit <http://creativecommons.org/licenses/by/4.0/>.

## 6. REFERENCES:

1. Hanawa, T. (2005). Roles of metals on regenerative medicine. *Journal of Hard Tissue Biology*, 14(2), 140-142.
2. Sygnatowicz, M., & Tiwari, A. (2009). Controlled synthesis of hydroxyapatite-based coatings for biomedical application. *Materials Science and Engineering: C*, 29(3), 1071-1076. <https://doi.org/10.1016/j.msec.2008.08.036>
3. Epple, M., Ganesan, K., Heumann, R., Klesing, J., Kovtun, A., Neumann, S., & Sokolova, V. J. J. C. (2010). Application of calcium phosphate nanoparticles in biomedicine. *Journal of Materials Chemistry*, 20(1), 18-23. <https://doi.org/10.1039/B910885H>
4. Hench, L. L. (1991). Bioceramics: from concept to clinic. *Journal of the American Ceramic Society*, 74(7), 1487-1510. <https://doi.org/10.1111/j.11512916.1991.tb07132.x>
5. LeGeros, R. Z. (1988). Calcium phosphate materials in restorative dentistry: a review. *Advances in dental research*, 2(1), 164-180. <https://doi.org/10.1177/08959374880020011101>
6. Geesink, R. G. (2002). Osteoconductive coatings for total joint arthroplasty. *Clinical Orthopaedics and Related Research (1976-2007)*, 395, 53-65.
7. Barrère, F., van der Valk, C. M., Dalmeijer, R. A., Meijer, G., van Blitterswijk, C. A., de Groot, K., & Layrolle, P. (2003). Osteogenicity of octacalcium phosphate coatings applied on porous metal implants. *Journal of Biomedical Materials Research Part A: An Official Journal of The Society for Biomaterials, The Japanese Society for Biomaterials, and The Australian Society for Biomaterials and the Korean Society for Biomaterials*, 66(4), 779-788. <https://doi.org/10.1002/jbm.a.10454>.
8. Brown, A., Zaky, S., Ray Jr, H., & Sfeir, C. (2015). Porous magnesium/PLGA composite scaffolds for enhanced bone regeneration following tooth extraction. *Acta biomaterialia*, 11, 543-553. <https://doi.org/10.1016/j.actbio.2014.09.008>
9. Jacobs, J. J., Skipor, A. K., Patterson, L. M., Hallab, N. J., Paprosky, W. G., Black, J., & Galante, J. O. (1998). Metal release in patients who have had a primary total hip

- arthroplasty. A prospective, controlled, longitudinal study. *JBJS*, 80(10), 1447-58.
10. Agins, H. J., Alcock, N. W., Bansal, M., Salvati, E. A., Wilson Jr, P. D., Pellicci, P. M., & Bullough, P. G. (1988). Metallic wear in failed titanium-alloy total hip replacements. A histological and quantitative analysis. *JBJS*, 70(3), 347-356.
  11. Slenters, T. V., Hauser-Gerspach, I., Daniels, A. U., & Fromm, K. M. (2008). Silver coordination compounds as light-stable, nano-structured and antibacterial coatings for dental implant and restorative materials. *Journal of Materials Chemistry*, 18(44), 5359-5362. <https://doi.org/10.1039/B813026D>
  12. Handbook, A. S. M. (1990). Properties and Selection: Nonferrous Alloys and Special-Purpose Materials (Asm Handbook) VOL. 2. *ASM: Almere, The Netherlands*, 1328.
  13. Copete, H., Vargas, F. A., López, E., Pérez, J. G., & Ríos, T. (2017). Improvement of the adhesion on hydroxyapatite coatings produced by oxyfuel thermal spray from results of numerical simulation. *DYNA: revista de la Facultad de Minas. Universidad Nacional de Colombia. Sede Medellín*, 84(203), 170 – 176 . <http://dx.doi.org/10.15446/dyna.v84n203.59201>
  14. Raines, A. L., Olivares-Navarrete, R., Wieland, M., Cochran, D. L., Schwartz, Z., & Boyan, B. D. (2010). Regulation of angiogenesis during osseointegration by titanium surface microstructure and energy. *Biomaterials*, 31(18),4909-4917. <https://doi.org/10.1016/j.biomaterials.2010.02.071>
  15. Ferrer Pacheco, M. Y., Moreno Téllez, C. M., & Vargas Galvis, F. (2018). Recubrimientos de zircona y alúmina por proyección térmica con llama: parámetros para obtener recubrimientos de alto punto de fusión.
  16. ASTM International. (2017). ASTM D3359-17: Standard test methods for rating adhesion by tape test. ASTM International. Doi:10.1520/D3359-17.
  17. Mahabole, M. P., Aiyer, R. C., Ramakrishna, C. V., Sreedhar, B., & Khairnar, R. S. (2005). Synthesis, characterization and gas sensing property of hydroxyapatite ceramic. *Bulletin of Materials Science*, 28, 535-545.
  18. Vaidhyanathan, B., & Rao, K. J. (1996). Rapid microwave-assisted synthesis of hydroxyapatite. *Bulletin of Materials Science*, 19, 1163-1165.
  19. Gómez-Morales, J., Torrent-Burgues, J., Boix, T., Fraile, J., & Rodríguez-Clemente, R. (2001). Precipitation of stoichiometric hydroxyapatite by a continuous method. *Crystal Research and Technology: Journal of Experimental and Industrial Crystallography*, 36(1), 15-26. [https://doi.org/10.1002/15214079\(200101\)36:1<15::AIDCRAT15>3.0.CO;2-E](https://doi.org/10.1002/15214079(200101)36:1<15::AIDCRAT15>3.0.CO;2-E)
  20. Yanovska, A. A., Stanislavov, A. S., Sukhodub, L. B., Kuznetsov, V. N., Illiashenko, V. Y., Danilchenko, S. N., & Sukhodub, L. F. (2014). Silver-doped hydroxyapatite coatings formed on Ti-6Al-4V substrates and their characterization. *Materials Science and Engineering: C*, 36, 215-220. <https://doi.org/10.1016/j.msec.2013.12.011>
  21. Wang, J. Y., Liu, Y. C., Lin, G. S., Chang, H. H., Li, Y. T., Yang, Y. C., ... & Tung, K. L. (2020). Flame-sprayed strontium and magnesium-doped hydroxyapatite on titanium implants for osseointegration enhancement. *Surface and coatings technology*, 386, 125452. <https://doi.org/10.1016/j.surfcoat.2020.125452>
  22. Stipniece, L., Salma-Ancane, K., Borodajenko, N., Sokolova, M., Jakovlevs, D., & Berzina-Cimdina, L. (2014). Characterization of Mg-substituted hydroxyapatite synthesized by wet chemical method. *Ceramics International*, 40(2), 3261-3267. <https://doi.org/10.1016/j.ceramint.2013.09.110>
  23. Hazaa, S. (2015). Effect of post-annealing on structural and optical properties of SnO2 thin Films deposited by Dc magnetron sputtering. *J. of Applied Physics IOSR-JAP*, 7, 59-63. 7.1 (2015): 59-63.
  24. Venkatesan, J., & Kim, S. K. (2010). Effect of temperature on isolation and characterization of hydroxyapatite from tuna (Thunnus obesus) bone. *Materials*, 3(10), 4761-4772. <https://doi.org/10.3390/ma3104761>
  25. Takács, J. (2005). Surface modification of metal implants with plasma sprayed layers. *J. Biomater*, 5, 54-59.

26. Pichugin, V. F., Tverdokhlebov, S. I., Surmenev, R. A., Shesterikov, E. V., Riabtseva, M. A., Kozelskaya, A. A., & Shulepov, I. A. (2006). Surface morphology and properties of calcium phosphate thin films formed by plasma of RF-magnetron discharge. *Phys. Basis. Radiation-Related Techno*, 49, 320-323.
27. Cavalli, M., Gnappi, G., Montenero, A., Bersani, D., Lottici, P. P., Kaciulis, S., ... & Fini, M. (2001). Hydroxy- and fluorapatite films on Ti alloy substrates: Sol-gel preparation and characterization. *Journal of Materials Science*, 36, 3253-3260.
28. Kokubo, T., & Takadama, H. (2006). How useful is SBF in predicting in vivo bone bioactivity?. *Biomaterials*, 27(15), 2907-2915. <https://doi.org/10.1016/j.biomaterials.2006.01.017>
29. Suchanek, K., Bartkowiak, A., Gdowik, A., Perzanowski, M., Kaç, S., Szaraniec, B., ... & Marszałek, M. (2015). Crystalline hydroxyapatite coatings synthesized under hydrothermal conditions on modified titanium substrates. *Materials Science and Engineering: C*, 51, 57-63. <https://doi.org/10.1016/j.msec.2015.02.029>
30. Kadhim, M. M., AlMashhadani, H. A., Hashim, R. D., Khadom, A. A., Salih, K. A., & Salman, A. W. (2022). Effect of Sr/Mg co-substitution on corrosion resistance properties of hydroxyapatite coated on Ti-6Al-4V dental alloys. *Journal of Physics and Chemistry of Solids*, 161, 110450. <https://doi.org/10.1016/j.jpcs.2021.110450>

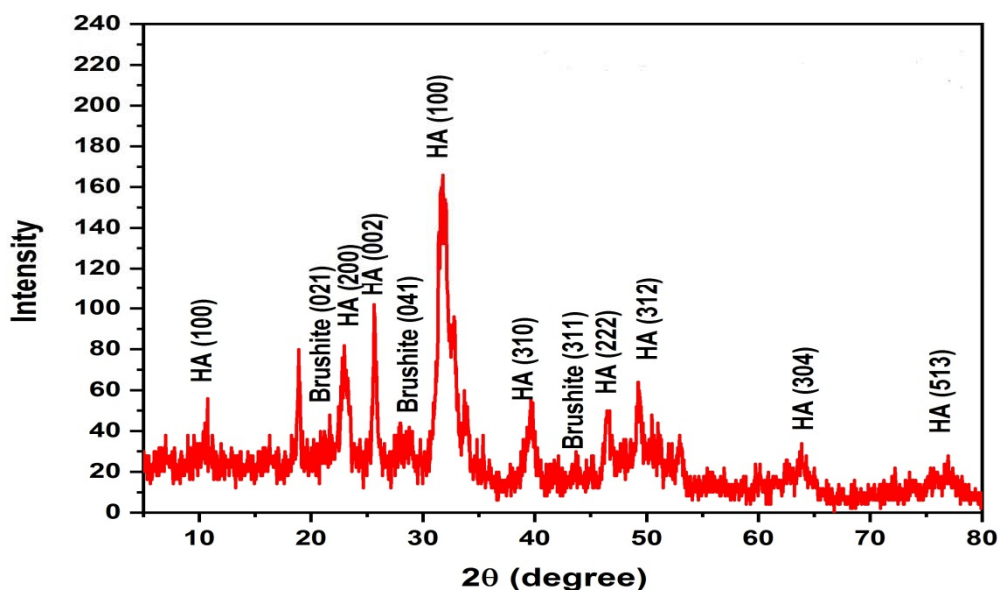


**Figure 1.** XRD pattern for titanium substrate coated with calcium phosphate.

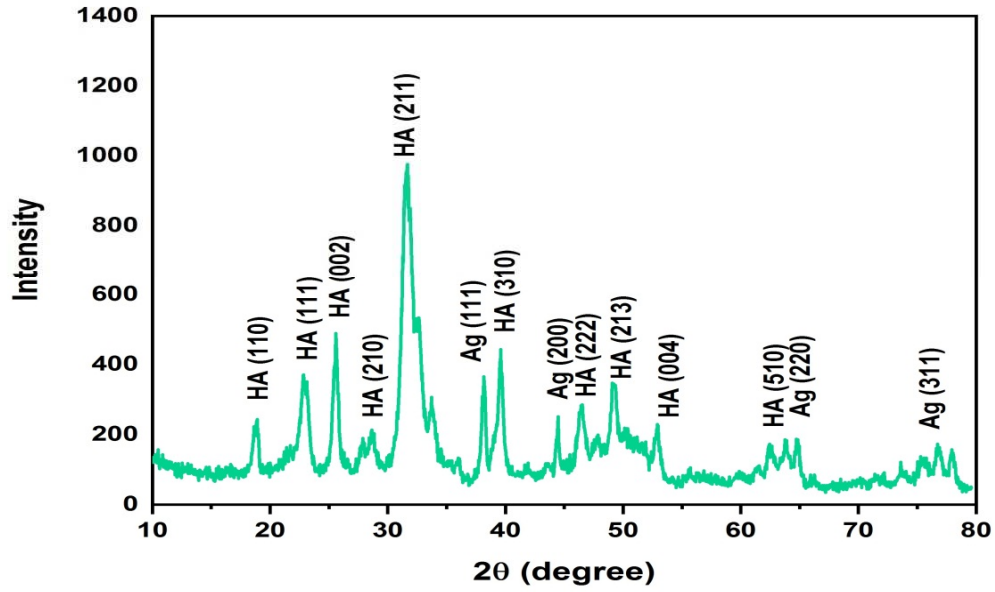


**Figure 2.** XRD pattern for titanium substrate coated with calcium phosphate and silver.

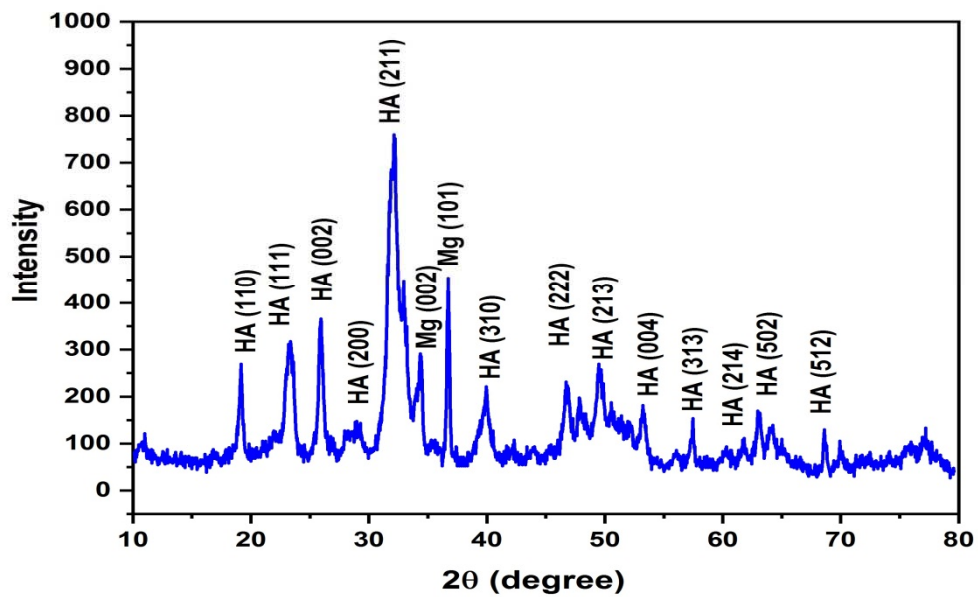


**Figure 3.** XRD pattern for titanium substrate coated with calcium phosphate and magnesium.

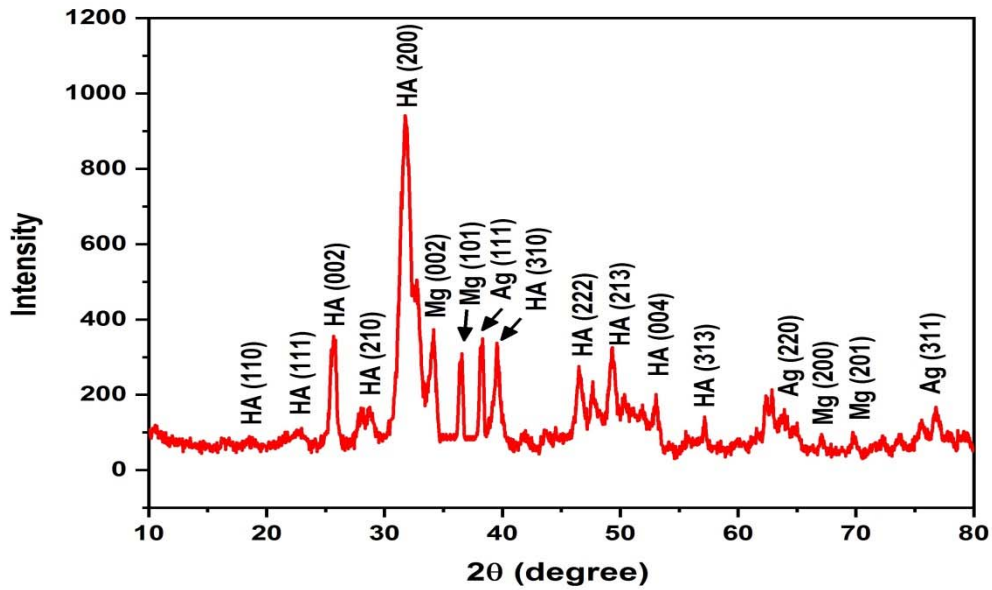


**Figure 4.** XRD pattern for titanium substrate coated with calcium phosphate, silver, and magnesium.

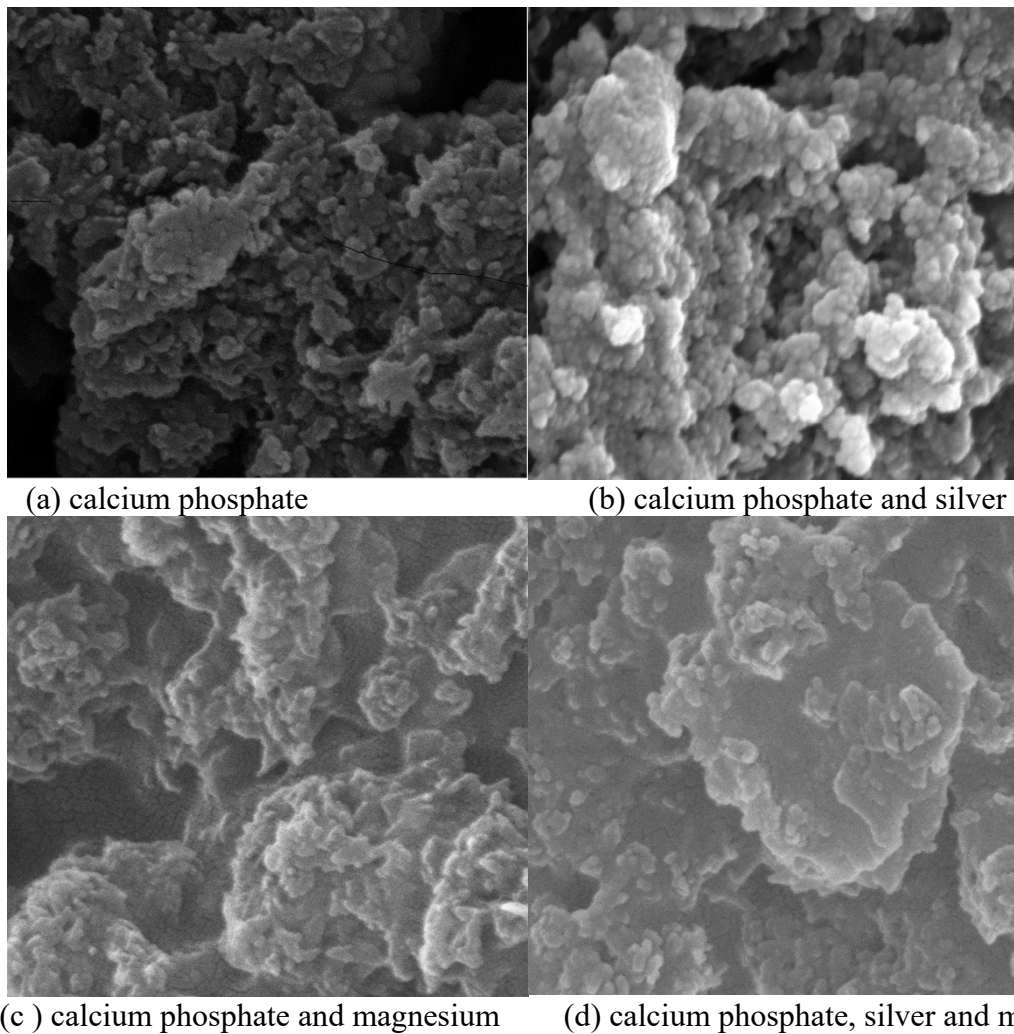


**Figure 5.** FE-SEM images for titanium substrate coated with (Cap, Cap Ag, Cap Mg, Cap Ag Mg).

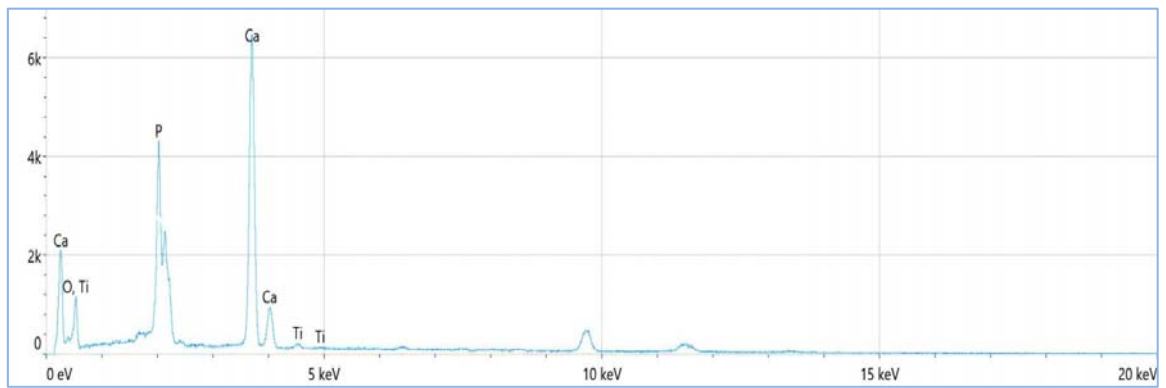


**Figure 6.** EDX analysis for Calcium Phosphate after deposition on Titanium substrate.

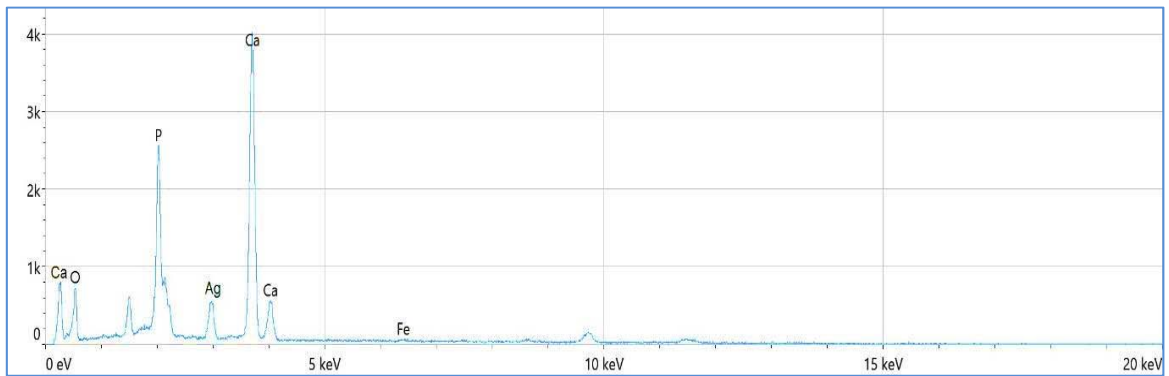


**Figure 7.** EDX analysis for Calcium Phosphate and silver after deposition on Titanium substrate.

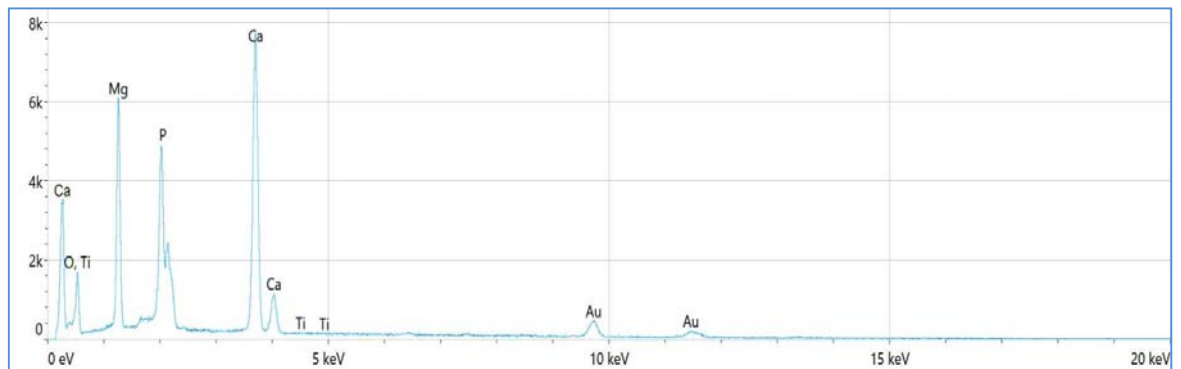


**Figure 8.** EDX analysis for Calcium Phosphate and magnesium after deposition on Titanium substrate.

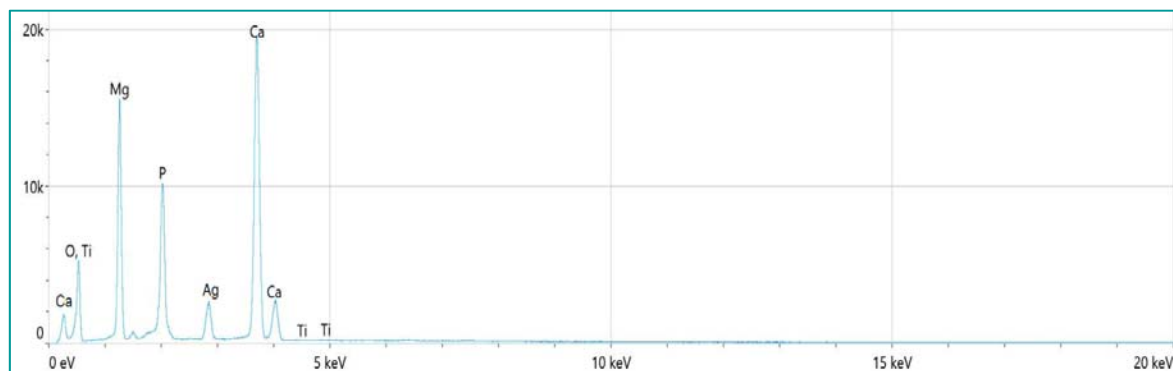


**Figure 9.** EDX analysis for Calcium Phosphate silver, and magnesium after deposition on Titanium substrate.

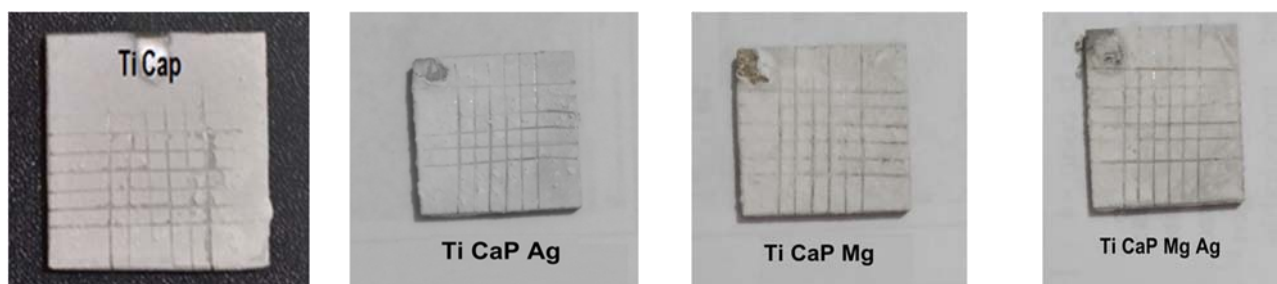


**Figure 10.** Adhesion test for titanium substrate coated with (Cap, Cap Ag, Cap Mg, Cap Ag Mg).